Phys. Status Solidi C **12**, No. 12, 1367–1371 (2015) / **DOI** 10.1002/pssc.201510135

physica status solidi c
www.pss-c.com
current topics in solid state physics

Local structure and photoluminescence properties of nanostructured $Zn_{1-x}Mn_xS$ material

Ana Laura Curcio[1], Maria Inês Basso Bernardi[2], and Alexandre Mesquita[*,1]

[1] Instituto de Geociências e Ciências Exatas, Universidade Estadual Paulista, Av. 24-A, 1515, 13506-900 Rio Claro, Brazil
[2] Instituto de Física de São Carlos, Universidade de São Paulo, Avenida Trabalhador São-Carlense 400, 13566-590 São Carlos, Brazil

Received 26 June 2015, revised 24 July 2015, accepted 26 July 2015
Published online 31 August 2015

Keywords zinc sulfide, manganese, ZnS:Mn, $Zn_{1-x}Mn_xS$, photoluminescence, nanostructure, X-ray absorption spectroscopy

* Corresponding author: e-mail mesquita@rc.unesp.br, Phone: +55 19 3526 9151, Fax: ++55 19 3526 9879

Zinc sulfide (ZnS) pure or doped has received remarkable attention because of fundamental properties, versatility and potential for several technological applications as luminescent material. In this study, the local structure and photoluminescence properties of nanostructured $Zn_{1-x}Mn_xS$ samples have been characterized. X-ray diffraction results show that ZnS:Mn samples crystallized completely without the presence of secondary phases and the diffraction patterns correspond to the cubic zinc blende. Theoretical and experimental XANES (X-ray absorption near edge structure) spectra at Zn K-edge suggest the incorporation of Mn atoms into the ZnS host and indicate the occurrence of Zn and S vacancies, which are confirmed by EXAFS (extended X-ray absorption fine structure) fit results. These vacancies can be related to a red-shift observed in the peak emission of photoluminescence spectrum for ZnS sample, which is centered at ~ 504 nm. As the Mn content increases, a yellow-orange emission centered at ~ 590 nm can be observed besides the blue-green emission, which is associated with the $^4T_1$–$^6A_1$ transition within the 3*d* shell of Mn^{2+}.

© 2015 WILEY-VCH Verlag GmbH & Co. KGaA, Weinheim

1 Introduction Nanocrystals have been extensively investigated in recent years due to their widespread applications in various devices such as sensors, solar cells, lasers, photocatalysts, photodetectors, infrared detectors, optical communication, colour television, flat panel display, phosphors, light emitting diodes, electroluminescent materials and other light-emitting materials [1-5]. This attracted attention is not only by new properties and its possible potential technological applications, but also the search for a better understanding of the physical and chemical processes that cause these new properties [4].

Nanocrystalline semiconductors have intermediate electronic properties between those of molecular structure and macrocrystalline solid, presenting a wide range of applications [1-5]. Among these materials, zinc sulfide (ZnS) pure or doped has received remarkable attention because of fundamental properties, versatility and potential for several technological applications [1, 2, 4]. ZnS is a typical II–VI compound semiconductor, with a direct band gap of 3.6 eV at room temperature and 40 meV as exciton binding energy, in addition to being a good luminescent material used in displays, sensors and lasers [2]. As a large band gap material, ZnS can easily host different transition metal ions as luminescent centers. Among these transition metal ions doped nanostructures, Mn^{2+} ions are attractive because of light-emitting properties for applications as efficient phosphors. This is due to the fact that doped Mn^{2+} ions provide good defect states for the excited electrons which are transferred from the conduction band to the *d* levels of these ions via $^4T_1 \rightarrow {}^6A_1$ transition [1]. This is observed as an orange emission.

Among different experiment methods to probe the structure of ZnS:Mn nanoparticles, X-ray absorption spectroscopy (XAS) has not been much used. As far as we know, few studies have addressed the local structure of ZnS material through XANES (X-ray absorption near edge structure) or EXAFS (extended X-ray absorption fine structure) spectra [6, 7]. In fact, XAS technique is a powerful tool for the investigation of local structures and provides meaningful additional structural information on materials [8]. Although the local structural data afforded by XAS are usually not sufficient to construct a whole structural model, they often provide valuable information about the local structural peculiarities [9]. These characteristics can be useful to interpret photoluminescence properties.

© 2015 WILEY-VCH Verlag GmbH & Co. KGaA, Weinheim

The purpose of this study is to probe the local structure of nanostructured $Zn_{1-x}Mn_xS$ semiconductor through XAS technique and to correlate to photoluminescence properties. In this study, ZnS:Mn samples were prepared by a solvothermal method, which has been shown to be an effective procedure to prepare doped or pure nanoparticles of ZnS [2, 10, 11]. These samples were characterized by X-ray diffraction, XANES and EXAFS spectra at Zn K-edge and photoluminescence spectroscopy techniques.

2 Experimental procedure The $Zn_{1-x}Mn_xS$ samples (x = 0.00, 0.01, 0.03, 0.05 as 0.10 – labeled as ZM100x) were prepared by solvothermal synthesis. This method is based on chemical co-precipitation method at room temperature [12]. The reaction conditions of solvothermal method, such as solution concentration, temperature and pH, have a strong influence on the reaction process but they present easy control low cost. The solvothermal process shows advantages over other preparation techniques include the stoichiometry control, purity and homogeneity of the particles prepared [11]. Zinc dichloride ($ZnCl_2$), manganese acetate tetrahydrate ($Mn(CH_3COO)_2.4H_2O$) and thiourea (H_2NCSNH_2) were used as reagents, which were diluted in ethylene glycol ($C_2H_6O_2$). Then, a sodium hydroxide solution (NaOH) were added and transferred separately in a sealed autoclave with volume of 110 ml. The precursor solutions were heated-treated by conducting heat under constant stirring at 140 °C during 30 min with a rate of 10 °C/min. After the synthesis, the autoclave was naturally cooled to room temperature. Then, each precipitated white powder was washed with warm deionized water for several times until attaining a neutral pH. The powder samples were dried at 80 °C for 12 hours.

The X-ray powder diffraction (XRD) patterns were measured at room temperature on a Rigaku Ultima 4 powder diffractometer with geometry θ-2θ, a rotating anode X-ray source (Cu-K_α radiation, λ = 1.542 Å), and a scintillation detector. The data were collected with a step size of 0.02°. The count time was 5 s per step.

Zn K-edge X-ray absorption spectra (9659 eV) were collected at the LNLS (National Synchrotron Light Laboratory) facility using the D04B-XAS1 beamline. The LNLS storage ring was operated at 1.36 GeV and 100-160 mA. These spectra were collected in transmission mode using an Si(111) channel-cut monochromator at room temperature. The samples thicknesses were optimized at each edge by the Multi-Platform Applications for XAFS (MAX) software package Absorbix code [13]. Normalized XANES and EXAFS spectra were extracted with the MAX-Cherokee code while the fitting procedure and comparison between experimental and theoretical EXAFS curves were conducted with the MAX-Roundmidnight package. The theoretical EXAFS spectra were calculated by the FEFF9 *ab initio* code [14] whose input files were issued from MAX-Crystalffrev software, which takes in account substitution disorder and random vacancies in the structure. In our work the relevant measure of the fit quality, the reduced statistical χ^2 is named QF (quality factor).

Photoluminescence spectra were collected with a Thermal Jarrel-Ash Monospec monochromator and a Hamamatsu R446 photomultiplier. The 350.7 nm exciting wavelength of a krypton ion laser (Coherent Innova) was used; the output of the laser was maintained at 200 mW. All measurements were taken at room temperature.

3 Results and discussion Figure 1 shows the X-ray diffraction patterns collected at room temperature for ZnS:Mn samples. The samples crystallized completely without the presence of secondary phases within the XRD detection limit. In good agreement with the literature, the diffraction planes of ZnS:Mn samples correspond to the cubic zinc blende (sphalerite) structure with *F*-43*m* space group [15]. It is observed significant broadening of the diffraction peaks which is ascribed to very small crystallite size. Scherrer's equation was used in order to evaluate the crystallite size values of all samples [16]. The average crystallite size was calculated using the full width at half maximum of (111) peaks from the XRD patterns for all samples depicted in Fig. 1. The calculated values are equal to 1.9, 1.8, 1.9, 1.9 and 1.5 nm for ZnS, ZM1, ZM3, ZM5 and ZM10, respectively, comparable to ZnS material prepared by the same method in a previous work [10].

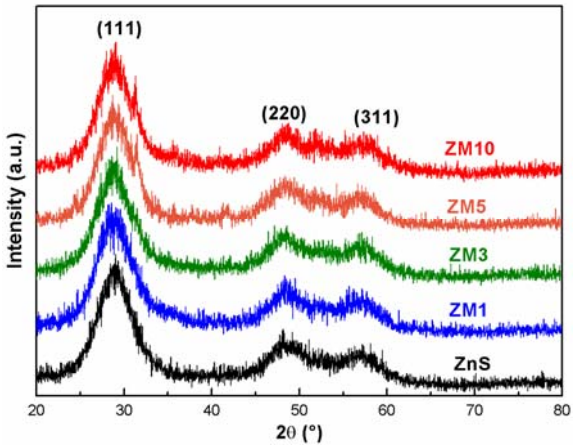

Figure 1 XRD patterns of ZnS and ZnS:Mn^2 samples with different Mn content.

The structure of $Zn_{1-x}Mn_xS$ samples was also characterized by XAS measurements. XANES spectra give information on the coordination symmetry and the valence of ions incorporated in a solid. The energy of the absorption edge shifts according to the valence of the absorbing ion, since the binding energy of bound electrons rises as the valence increases. Also, the shape of the absorption edge depends on the unfilled local density of states and the coordination symmetry of the absorbing element. The spectrum at the Zn *K*-edge is characteristic of the electron transition from the 1*s* state to empty 4*p* states.

© 2015 WILEY-VCH Verlag GmbH & Co. KGaA, Weinheim

In Fig. 2 XANES spectrum at Zn *K*-edge is shown for the ZnS standard compound. This spectrum exhibits similar *K*-edge white line shapes and XANES features to those previously reported for tetrahedral coordinated ZnS [17, 18]. Calculated XANES spectrum for ZnS (light green line) compound using *ab initio* FEFF code [14] is also shown in this figure. The input files for FEFF code with cluster radius of 6.0 Å were generated using CRYSTALFREV software [13] and, as can be seen in this figure, calculated XANES spectra reproduce satisfactorily the experimental spectra.

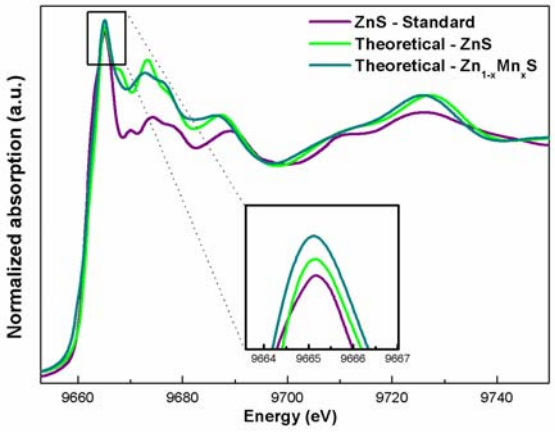

Figure 2 Experimental XANES spectra of ZnS standard and theoretical XANES spectra for pure ZnS and $Zn_{1-x}Mn_xS$ sample. The lower-rigth inset shows details of white line of these spectra.

Mn atoms were also randomly incorporated at Zn sites of ZnS structure forming $Zn_{1-x}Mn_xS$ with x = 0.10 and the calculated XANES spectra is also shown (dark green line). As can be seem in the inset, the intensity of white line increases as Zn atoms are substituted by Mn atoms. This increase can be related to the fact that The K-edge XANES here reproduces the density distribution of the unoccupied *p*-like states around Zn atoms. Reduction of the Zn atomic content causes an increased localization of the Zn *p*-like states and, in consequence, sharper resonances [7].

Figure 3 shows the normalized Zn K-edge XANES spectra of ZnS standard, ZnS and ZnS:Mn nanostructured powders. The spectra of nanostructured samples are almost identical, showing that the Zn environment was not significantly affected by the Mn content increasing. The upper-left inset shows the only difference between these spectra: the intensity of white-line peak increases for ZnS:Mn samples compared to ZnS sample. This result is in agreement with our calculated XANES spectra and indicates undoubtedly that Mn^{2+} ion are incorporated at Zn sites in ZnS structure.

On the other hand, the XANES spectra of nanostructured ZnS:Mn samples are considerable different to the spectrum of ZnS standard. The intensity of white line is lower and all the features in XANES region are less discernible for ZnS:Mn samples. In order to assess these characteristics, theoretical XANES spectrum was obtained considering in the calculation only the first shell of four S atoms around absorber Zn atom. The lower-right inset in Fig. 3 shows this spectrum compared to the XANES spectrum of nanostructured ZnS and, as can be observed, this theoretical spectrum agrees well with the experimental one. Although the main features of the Zn K-edge structure (i.e., the three peaks between 9660 and 9700 eV) are well reproduced with the atoms of the first coordination sphere [7], the XANES spectrum calculated suppressing the second shell with 12 Zn atoms shows good agreement to experimental spectra.

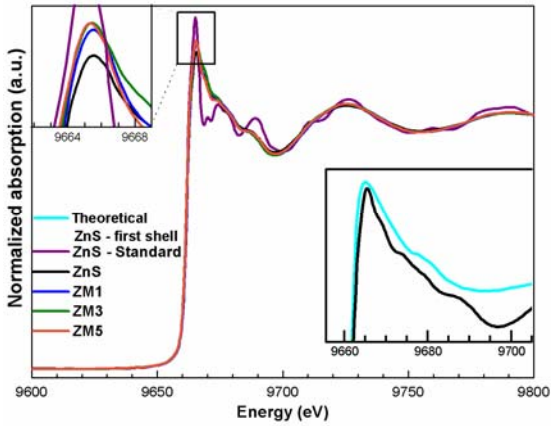

Figure 3 XANES spectra for ZnS:Mn samples. The upper-left inset shows details of white line and the lower-right inset shows theoretical XANES calculated with one shell of S neighbors around Zn absorber atom.

The short-range structural data provided by extended X-ray absorption fine structure (EXAFS) offers an element-specific insight, giving quantitative information about the number, position and identity of atoms surrounding the absorbing element as well as structural disorder within the coordination spheres. In order to obtain quantitative information of the local structure around Zn atoms, Fourier transform curves were then back Fourier transformed between 1.0 and 5.0 Å to obtain the experimental EXAFS spectra to fit using a theoretical model calculated from FEFF9 code and crystallographic information according the XRD measurements.

The fitted k^3 weighted Fourier transforms of the ZnS standard and nanostructured ZnS:Mn samples are shown in Fig. 4. The intensity of the modulus of Fourier transform decreases for nanostructured samples compared to ZnS standard, mainly in the region between 3.0 and 5.0 Å. In all fits, we considered single scattering paths corresponding to the first (four S atoms), second (12 Zn atoms) and third (12 S atoms) shells around Zn absorber atom according to the cubic zinc blende structure with *F*-43*m* space group. The number of free parameters was kept smaller than the number of independent points, which is defined as $N_{ind} = 2\Delta R\Delta k/\pi$, where ΔR is the width of the *R*-space filter windows and Δk is the actual interval of the fit in the *k*-space [19]. The reliability of the fit, determined by a quality fac-

© 2015 WILEY-VCH Verlag GmbH & Co. KGaA, Weinheim

tor (QF) [19], coordination number (N), interatomic distances (R) and Debye-Waller factor (σ^2) relative to the fits are shown in Table 1.

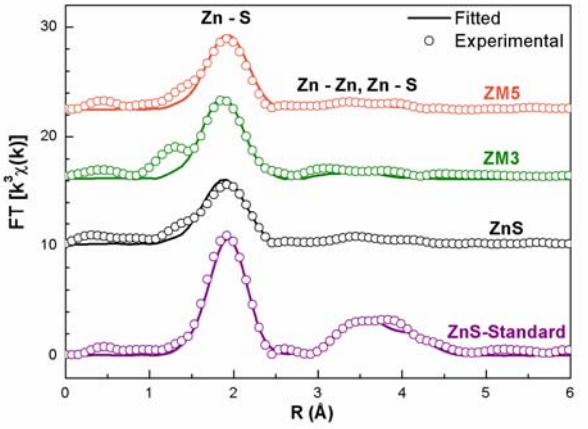

Figure 4 Fitted and experimental k^3-weighted Fourier transforms of the ZnS:Mn samples.

Table 1 Results of fits to the EXAFS spectra of Zn K-edge EXAFS simulation results. R is the distance from the central atom, N is the average coordination number, σ^2 the Debye-Waller factor and QF the quality factor [19].

Sample	Shell	R (Å)	N	σ^2 (Å^2)	QF
ZnS standard	Zn-S_I	2.33(1)	4.2(8)	0.0027(19)	1.52
	Zn-Zn_I	3.83(2)	10.2(1.2)	0.0144(27)	
	Zn-S_{II}	4.48(1)	7.7(1.4)	0.0027(19)	
ZnS	Zn-S_I	2.30(1)	3.8(5)	0.0067(18)	1.41
	Zn-Zn_I	3.77(2)	6.1(2.1)	0.0202(47)	
	Zn-S_{II}	4.42(1)	0.6(1.3)	0.0067(18)	
ZM3	Zn-S_I	2.30(1)	4.0(4)	0.0060(12)	2.08
	Zn-Zn_I	3.73(4)	4.5(1.4)	0.0180(79)	
	Zn-S_{II}	4.69(6)	0.4(1.1)	0.0060(12)	
ZM5	Zn-S_I	2.30(1)	4.1(5)	0.0061(15)	2.32
	Zn-Zn_I	3.83(2)	2.1(1.7)	0.0224(138)	
	Zn-S_{II}	4.48(4)	0.8(1.6)	0.0061(15)	

According to the structural model, the more intense peak, between 1.5 and 2.5 Å in the Fourier transforms corresponds to single scattering interaction between the first S atoms around absorber atom. The single scattering interactions relative to Zn-Zn and Zn-S (beyond the first S neighbors) paths correspond to the peaks and shoulders observed between 3.0 and 5.0 Å. This region also includes multiple scattering paths such as Zn-S-S, Zn-S-Zn-S, Zn-S-S-S and Zn-Zn-S interactions. As can be seen in Table 1, the obtained QF factors indicate the reliability of the fits, which is confirmed by the comparison of the fitted (lines) and experimental (symbols) data in Fig. 4. No alterations within the uncertainty are observed in the distance between each shell and Zn absorber atom. On the other hand, Debye-Waller factor values exhibit larger values for ZnS:Mn powders prepared by solvothermal method, which would be expected for nanostructured materials. Moreover, the average coordination number decreases considerably for nanostructured samples in second and third shells. Thus, the fits of EXAFS spectra indicate a significantly number of vacancies in both S and Zn sites for ZnS nanoparticles, which suggest the presence of imperfectness in the crystal lattice. As the average crystallite size is only ~2 nm according our XRD measurements, a large amount of the atoms should be placed at the boundary of particles resulting in a lower number of neighbours [20]. This fit result is in good agreement with theoretical XANES spectrum which considers only the first shell around Zn atoms to generate all the features, as shown in Fig. 3.

Figure 5 presents the photoluminescence (PL) spectra for pure and doped ZnS:Mn samples. As can be seen in this figure, the spectrum for ZnS sample is highly asymmetrical, broadened and centred at ~ 504 nm, with multiple peaks indicating the involvement of different luminescence centers in the radiative processes. This spectrum exhibits similar features compared to that one reported by Ferrer et al. [10], although reports from different groups have shown PL spectra of ZnS centred at lower wavelengths [1, 2, 21-24].

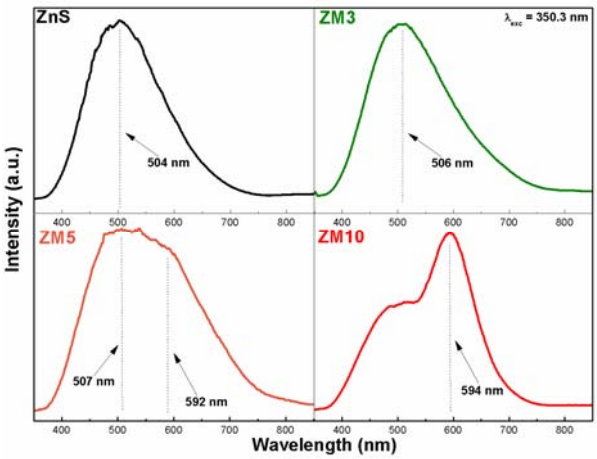

Figure 5 Photoluminescence spectra for ZnS:Mn samples.

According to Kripal et al., ZnS presents four blue-green emissions centred at 417, 446, 480 and 520 nm which arise due to interstitial S lattice defects, interstitial Zn lattice defects, S vacancies and Zn vacancies, respectively [1]. Since S ions have larger ionic radii (1.7 Å) than that of Zn ions (0.74 Å), interstitial S produces more strain in the ZnS lattice and thus the electron levels due to this site will have smaller binding energy [1]. Therefore, interstitial S energy levels must be closer to valence band than the interstitial Zn energy levels to the conduction band. Similarly S vacancy states are closer to conduction band edge than Zn vacancies states to the valence band edge [1]. Thus, the red-shift observed in Fig. 5 for nanostructured ZnS sample could be related to the presence of S and Zn vacancies, as shown in XAS results.

© 2015 WILEY-VCH Verlag GmbH & Co. KGaA, Weinheim

As the Mn content increases, a yellow-orange emission centered at ~ 590 nm can be observed besides the blue-green emission, which is associated with the $^4T_1$–$^6A_1$ transition within the 3*d* shell of Mn^{2+}. According to Bhargava and Gallagher [25], the yellow-orange emission is attributed to an efficient energy transfer from the ZnS host to Mn^{2+} ions facilitated by the mixed electronic states [1]. When Mn^{2+} ions are incorporated into the ZnS lattice and substitute for the cation sites, the mixing between the *s*–*p* electrons of the host ZnS and the *d* electrons of Mn^{2+} occurs and makes the forbidden transition of $^4T_1$–$^6A_1$ partially allowed, resulting in the characteristic emission of Mn^{2+} [1, 25].

Moreover, Sooklal et al. [26] studied the effect of the location of Mn^{2+} on the photophysics of ZnS nanoparticles. They found that Mn^{2+} incorporation into the ZnS lattice lead to the orange emission while ZnS with surface-bound Mn^{2+} yielded the ultraviolet emission [1]. As a comparison with Fig. 5, it can be suggested that the Mn^{2+} ions are incorporated into the ZnS nanoparticles. As stated earlier, theoretical and experiment XANES spectra also indicate this substitution.

4 Conclusions In this study, the local structure and photoluminescence properties of nanostructured $Zn_{1-x}Mn_xS$ samples have been characterized. XRD results show that ZnS:Mn samples crystallized completely without the presence of secondary phases and the diffraction patterns correspond to the cubic zinc blende (sphalerite) structure with *F*-43*m* space. Theoretical and experimental XANES spectra at Zn K-edge suggest the incorporation of Mn atoms into the ZnS host and indicate the occurrence of Zn and S vacancies, which are confirmed by EXAFS fit results. These vacancies can be related to a red-shift observed in the peak emission of photoluminescence spectrum for ZnS sample, which is centered at ~ 504 nm. As the Mn content increases, a yellow-orange emission centered at ~ 590 nm can be observed besides the blue-green emission, which is associated with the $^4T_1$–$^6A_1$ transition within the 3*d* shell of Mn^{2+}.

Acknowledgements The authors thank FAPESP (through project 2013/12993-4) and CNPq funding agencies. The research was partially carried out at LNLS National Laboratory of Synchrotron Light (proposal number XAFS1-17750), Brazil.

References

[1] R. Kripal, A. K. Guptaa, S. K. Mishrab, R. K. Srivastavab, A. C. Pandeyc, and S.G. Prakashb, Spectrochim. Acta A **76**, 523 (2010).
[2] J. Caoa, J. Yangc, Y. Zhangc, L. Yangc, Y. Wangc, M. Wei, Y. Liuc, M. Gaoc, X. Liuc, and Z. Xied, J. Alloys Compd. **486**, 890 (2009).
[3] S. Kar and S. Biswas, J. Phys. Chem. C **112**, 11144 (2008).
[4] V.L. Klimov, S.A. Lvanov, and J. Nanda, Nature **447**, 441 (2007).
[5] T. Toyama, T. Hama, and D. Adachi, Nanotechnology **20**, 055203 (2009).
[6] B. Gilbert, B. H. Frazer, H. Zhang, F. Huang, J. F. Banfield, D. Haskel, J. C. Lang, G. Srajer, and G. De Stasio, Phys. Rev. B **66**, 245205 (2002).
[7] K. Ławniczak-Jabłonska, R. J. Iwanowski, Z. Gołacki, A. Traverse, S. Pizzini, A. Fontaine, I. Winter, and J. Hormes, Phys. Rev. B **53**, 1119 (1996).
[8] V.A. Shuvaeva, I. Pirog, Y. Azuma, K. Yagi, K. Sakaue, H. Terauchi, I.P. Raevskii, K. Zhuchkov, and M. Y. Antipin, J. Phys.: Condens. Matter **15**, 2413 (2003).
[9] V.A. Shuvaeva, D. Zekria, A. M. Glazer, Q. Jiang, S.M. Weber, P. Bhattacharya, and P. A. Thomas, Phys. Rev. B **71,** 174114 (2005).
[10] M. M. Ferrer, Y. V. B. de Santana, C. W. Raubach, F. A. La Porta, A. F. Gouveia, E. Longo, and J. R. Sambrano J. Mol. Model. **20**, 2375 (2014).
[11] M. M. Ferrer, Y. V. B. de Santana, C. W. Raubach, J. R. Sambrano, and E. Longo, Curr. Phys. Chem. **3**, 413 (2013).
[12] N. Herron, Y. Wang, and H. Eskert., J. Am. Chem. Soc. **112**, 1322 (1990).
[13] A. Michalowicz, J. Moscovici, D. Muller-Bouvet, and K. Provost, J. Phys.: Conf. Series **190**, 012034 (2009).
[14] A. L. Ankudinov, B. Ravel, S. D. Conradson and J. J. Rehr, Phys. Rev. B **58**, 7565 (1998).
[15] B. K. Agrawal, P. S. Yadav, and S. Agrawal, Phys. Rev. B **50**, 1481 (1994).
[16] M. P. Klug and L. E. Alexander, X-ray Diffraction Procedure for Polycrystalline and Amorphous Materials (Wiley-Interscience Publication, New York, 1974).
[17] B. Gilbert, B. H. Frazer, H. Zhang, F. Huang, J. F. Banfield, D. Haskel, J. C. Lang, G. Srajer, and G. De Stasio, Phys. Rev. B **66**, 245205 (2002).
[18] K. Ławniczak-Jabłonska, R. J. Iwanowski, Z. Gołacki, A. Traverse, S. Pizzini, and A. Fontaine, Physica B **208-209**, 497 (1995).
[19] S. S. Hasnain, Report on the International Workshops on Standards and Criteria in XAFS, in: X-ray Absorption Fine Structure: Proceedings of the VI International Conference on X-ray Absorption Fine Structures (Ellis Horwood, New York, 1991).
[20] G.-C. Yi, Semiconductor Nanostructures for Optoelectronic Devices Processing, Characterization, and Applications (Springer, Heidelberg, Dordrecht, London, New York, 2012).
[21] N. Murase, R. Jagannathan, Y. Kanematsu, M. Watanabe, A. Kurita, K. Hirata, T. Yazawa, and T. Kushida, J. Phys. Chem. B **103**, 754 (1999).
[22] W. Z. Zhang, J. L. Shi, H. R. Chen, Z. L. Hua, and D. S. Yan, Chem. Mater. **13**, 648 (2001).
[23] Y. C. Li, X. H. Li, C. H. Yang, and Y. F. Li, J. Phys. Chem. B **108**, 16002 (2004).
[24] R. Viswanath, H. S. B. Naik, G. S. Y. Kumar, P. N. P. Kumar, G. A. Kumar, and R. Praveen, J. Lumin. **153**, 446 (2014).
[25] R. N. Bhargava and D. Gallagher, Phys. Rev. Lett. **72**, 416 (1994).
[26] K. Sooklal, B. S. Cullum, S. M. Angel, and C. J. Murphy, J. Phys. Chem. **100,** 4551 (1996).

© 2015 WILEY-VCH Verlag GmbH & Co. KGaA, Weinheim